Scientific Research and Essays Vol. 7(29), pp. 2641-2655, 30 July, 2012
Available online at http://www.academicjournals.org/SRE
DOI: 10.5897/SRE12.375
ISSN 1992-2248 ©2012 Academic Journals

Full Length Research Paper

Digital image processing techniques demonstrating the anomalous nature of the radiocarbon dating sample area of the Shroud of Turin

John M. Morgan, III

Geospatial Research and Education Laboratory, Department of Geography and Environmental Planning, Towson University, 8000 York Road, Baltimore, Maryland 21252-0001 USA. E-mail: jmorgan@towson.edu. Tel: 410-704-2964. Fax: 410-704-4702.

Accepted 12 July, 2012

This article reports on the use of digital image processing techniques to analyze an ultraviolet-fluorescence photograph of the area of the Shroud of Turin where the radiocarbon dating samples were taken. Results of this analysis demonstrate the anomalous nature of the radiocarbon data sample area. The techniques employed in this investigation are those used by the land remote sensing community for the analysis of multispectral imagery. The techniques included extraction of the RGB bands from a digital version of the ultraviolet-fluorescence photograph, use of principal components analysis for statistical compression of the RGB bands, calculation of z-score values using the first component of the principal components analysis, unsupervised classification of the RGB bands via K-MEANS clustering, and image segmentation. These techniques were also used to determine whether the area where the radiocarbon dating samples were taken exhibited any spectral anomalies. A one sample z-test demonstrated that there is a statistically significant difference between the mean z-scores for the four radiocarbon data samples and the mean z-score for a sample area of the Shroud with representative ultraviolet fluorescence. Results of the investigation suggest there is a new set of non-destructive techniques available to support further analysis of the Shroud. Recommendations are made regarding the need for high spatial resolution multispectral imagery and a Shroud coordinate system for mapping Shroud features.

Key words: Brightness values, digital image processing, image segmentation, K-MEANS clustering, principal components analysis, radiocarbon dating sample area, Shroud of Turin, ultraviolet-fluorescence photograph.

INTRODUCTION

The following are the results of an investigation of the ultraviolet-fluorescence (UV-F) photograph of the radiocarbon (C-14) dating sample area of the Shroud of Turin (TS). The UV-F photograph, which was taken by Vernon D. Miller of the Brooks Institute of Photography in Santa Clara, California in 1978, was available for download in the Links section of the ShroudScience Group page on yahoo.com.

The digital photograph was verified by Giulio Fanti (Department of Mechanical Engineering, Padua University) as the original UV-F photograph taken of the lower ventral corner of the TS in 1978. According to the late Raymond N. Rogers: “The area where the radiocarbon sample was obtained had been photographed in 1978 with an ultraviolet source… . While making the UV photographs, the source was heavily filtered to exclude visible light and the camera was heavily filtered to exclude any effect of the UV on the film. All that appears on the film is the result of pure fluorescence. All fluorescence is a result of the chemical composition of the material” (Rogers, 2004).The TS, believed by many to be burial cloth of Jesus of Nazareth, has been described as the most analyzed piece of linen in history.

The purpose of this investigation was to determine whether digital image processing software and techniques commonly used by the land remote sensing community for the processing of multispectral imagery collected by airborne and spaceborne sensors could be

used to process the brightness values in the UV-F photograph. The investigation also attempted to determine whether any spectral anomalies in the C-14 sample area of the TS could be identified using the UV-F photograph. This is not the first time images of the TS have been analyzed using digital image processing techniques. The Shroud of Turin Research Project (STURP) collected "spectrally-resolved Quad-Mosaic photography" during its investigation of the TS in 1978 (Avis et al., 1982). The Quad-Mosaic images were processed in an effort to display the surface chemical composition of the TS (Avis et al., 1982).

MATERIALS AND METHODS

After downloading the photographic image (14C-UV.jpg), the jpeg file was input to Corel Paint Shop Pro. The dimensions of the image (including the white border to the right and bottom of the image) were 603 columns by 555 rows. The image, which measures 51.05 by 46.99 mm (2.01 by 1.85 inches), was scanned at a resolution of 118.11 pixels per centimeter (300 pixels per inch) and has a pixel depth of 16 million colors. Pixel dimensions (width and length) were calculated to be 0.0847 by 0.0847 mm (0.0033 by 0.0033 inches).

Corel Paint Shop Pro was used to perform initial processing of the UV-F photograph. Specifically, the image's color depth was decreased to 64K colors. Also, the 24-bit RGB image was separated into its constituent 8-bit blue, green, and red bands. Finally, the 24-bit RGB UV-F image, along with the 8-bit blue, green, and red images extracted from the 24-bit RGB bands, were "clipped" (cropped) to remove the white border. The dimensions of the clipped images were 288 columns by 317 rows (91,296 total pixels).

The clipped images were input to the Taiga edition of IDRISI by Clark University (Clark Labs, IDRISI GIS and Image Processing Software, 2011), the image processing and geographic information systems (GIS) software was used for this investigation. These files included the 24-bit RGB UV-F image (Figure 1), along with the 8-bit blue, green, and red bands (Figures 2, 4 and 6), respectively. Histograms were generated for the 8-bit blue, green, and red bands (Figures 3, 5 and 7), respectively. The histograms demonstrate that each of the three bands derived from the 24-bit RGB UV-F image records a unique pattern of brightness values. In addition to apparent visual differences in the three histograms, the means of the brightness values of the three histograms were 68.783, 115.882 and 165.854, respectively.

A principal components analysis (PCA) was performed on the blue, green, and red bands derived from UV-F image. PCA, a linear transformation technique related to Factor Analysis, is a digital image processing technique used for data compression. In the forward process, PCA produces a new set of images (components) that are uncorrelated with each other and explain progressively less of the variance found in the original set of bands. The options selected for the PCA included calculating the covariances directly and using unstandardized variables (variance/covariance matrix) in a forward transformation of the original bands. The first component of the PCA (Figure 8) explains 97.41% of the variance found in the blue, green, and red bands derived from the UV-F image.

Benford and Marino (2008) included in their paper the location where the samples were taken for radiocarbon dating. A digital version of this graphic (Figure 9) was downloaded from the Shroud of Turin Skeptical Spectacle Web site (http://www.skepticalspectacle.com/carbon1400.htm). This graphic was converted to an 8-bit jpeg using Corel Paint Shop Pro, imported to IDRISI, and then resampled to fit the clipped version of the UV-F image using IDRISI. Resampling is used to register image data in one grid system to that of a different grid system covering the same area. This technique uses polynomial equations to establish a "rubber sheet" transformation of the image. Resampling is also described as a "control point warp" in remote sensing literature. The image was resampled using 10 control points with a linear (first order) polynomial fit and nearest neighbor interpolation.

The resampled Benford and Marino image was exported from IDRISI as a geotiff file and then imported to the ArcGIS 10, GIS software from Environmental Systems Research Institute in their paper (http://www.esri.com). ArcGIS was used to "heads up" digitize the boundaries of C-14 sample area from the resampled image. The results of this process were stored in Esri vector (shapefile) format. The ArcGIS shapefile was then imported to IDRISI and rasterized to the resolution of the UV-F image. A vector version of the C-14 sample area can be overlayed on any of the raster images to show the exact location where radiocarbon dating samples were taken (Figure 10).

Standard scores (z-scores) were calculated for the first component of the PCA to determine if any spectral anomalies exist in the C-14 sample area. As Rogers and Arnoldi noted: "The radiocarbon sample area is darker than normal, a fact that is not the result of image color or scorching. The cloth is much less fluorescent in that area, brightening into more normal fluorescence to the right. The photograph proves that the radiocarbon area has a different chemical composition than the main part of the cloth, and it is truly anomalous." (Rogers and Arnoldi, 2000).

To calculate standard scores for the first component of the PCA, a 100 by 100 pixel sample area was selected at random from the right portion of the UV-F image noted by Rogers and Arnoldi as having "more normal fluorescence." The pixel coordinates (column/row) for the upper-left, upper-right, lower-right, and lower-left corners of the sample area were 172/38, 271/38, 271/137, and 172/137, respectively. The z-score sample area is shown in Figure 11. This sample area represented an area of 10,000 pixels, or 10.95% of the total number of pixels for the clipped images used in this investigation. Selected statistics were extracted from the first component of the PCA for the z-score sample area (Table 1).

IDRISI's Image Calculator was used to calculate the standard score (z-score) for each pixel in the first component of the PCA (Figure 12). Images can be used as variables in an equation using Image Calculator. To calculate z-scores and create the z-score image (Figure 12), the first component of the PCA was used as an image in the z-score equation in Image Calculator. Selected statistics were extracted from the z-score image for the four C-14 sample areas and the z-score sample area (Table 2).

The selected statistics were also extracted for the Retained area shown in Figure 9, and for the unnamed area between Areas 1 through 4 and the Retained area and the seam where the patch was joined with the TS and the Raes fragment. The selected statistics for the Retained area were -6.4822 (minimum value), -2.7028 (maximum value), -5.1312 (mean) and 0.5109 (standard deviation). The selected statistics for the unnamed area were -7.6290 (minimum value), -1.4805 (maximum value), -5.6225 (mean) and 0.5978 (standard deviation).

STURP researchers observed that "if the chemicals were spectrally differentiated, the multispectral classification process could provide a map of chemical composition throughout the Shroud image" (Avis et al., 1982). The primary purpose of digital image processing of remotely sensed images is to extract information about land or water areas based on the variability of brightness values of reflected and emitted energy captured by the remote sensing instrument (Jensen, 1996). Two techniques are available to the land remote sensing analyst to classify brightness values from multispectral image: 1) supervised classification; and 2) unsupervised classification. In supervised classification, the analyst develops "training areas" that identify a particular type of land or water feature. The image processing software uses the training area data to classify an image to show whatever features are being

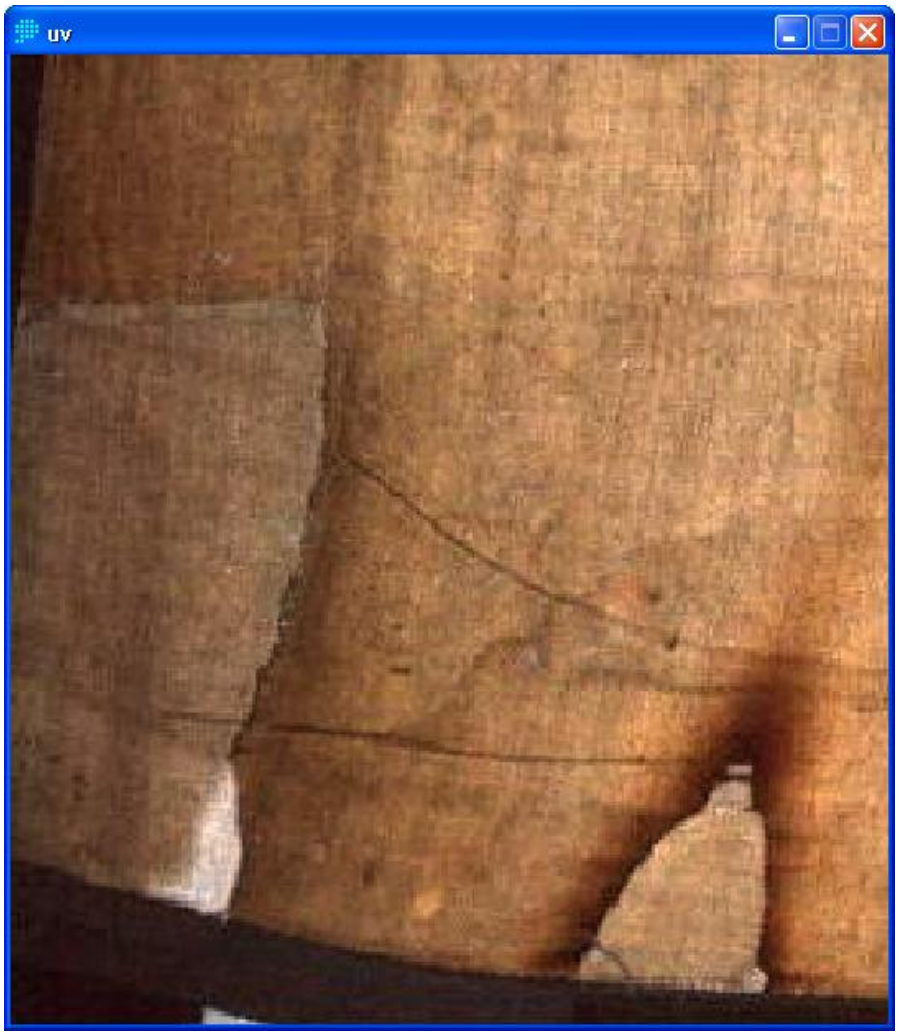

Figure 1. Clipped version of the UV-F image (14C-UV.jpg).

mapped based on the spectral signatures of the training areas. In unsupervised classification, the image processing software segments multispectral data into *n* categories of like spectral response using one of several classification algorithms. The analyst can then assign the categories to specific features based on *a priori* knowledge of the study area.

For this investigation, an unsupervised classification was performed on the first component of the PCA using IDRISI's K-MEANS classifier. K-MEANS is a method of cluster analysis that aims to partition *n* observations into *k* clusters in which each observation belongs to the cluster with the nearest mean. The K-MEANS classification of the first component of the PCA was based on a random seed cluster centroid initialization rule, a maximum of 16 output clusters, and a maximum of 500 iterations. The percentage of migrating pixels was set to be less than or equal to 1.0% and clusters with proportions less than or equal to 1.0% were merged. K-MEANS begins by initializing *k* centroids (means), then assigns each pixel to the cluster whose centroid is nearest, updates the cluster centroids, then repeats the process until the *k* centroids are fixed. The 16 output cluster maximum is the default setting for IDRISI's K-MEANS classifier. The result of the K-MEANS clustering is shown in Figure 13. In addition to the results of the statistical test described below, Figure 13 provides visual confirmation of the anomalous nature of the C-14 sample area. Similar results were obtained by setting the maximum number of output clusters to 8 and 24.

IDRISI was also used to segment the first component of the PCA (Figure 10). Segmentation groups adjacent pixels into image "objects" (segments) according to their spectral similarity. An object, then, is a spatial unit that differs from its surroundings based on values within an image. Segmentation employs a watershed delineation approach to partition input imagery based on their variance. A derived variance image is treated as a surface image allocating pixels to particular objects based on variance similarity. After segmentation, the analyst can identify selected image objects as training areas for a supervised classification of the image, or use objects to calculate statistics for image values. Segmentation is a relatively new technique for extracting information from remotely sensed imagery.

Pixel segmentation of the first component of the PCA was based on a window width of 3, a weight mean factor of 0.5, a weight variance factor of 0.5, and a similarity tolerance of 20. Other similarity variances were also tested. The results of the segmentation with a similarity tolerance of 5 (Figure 14) represented an appropriate balance between the scale of the image and the size of the image objects.

Using IDRISI, the values in the z-score image (Figure 12) were transformed to positive numbers using the absolute value function.

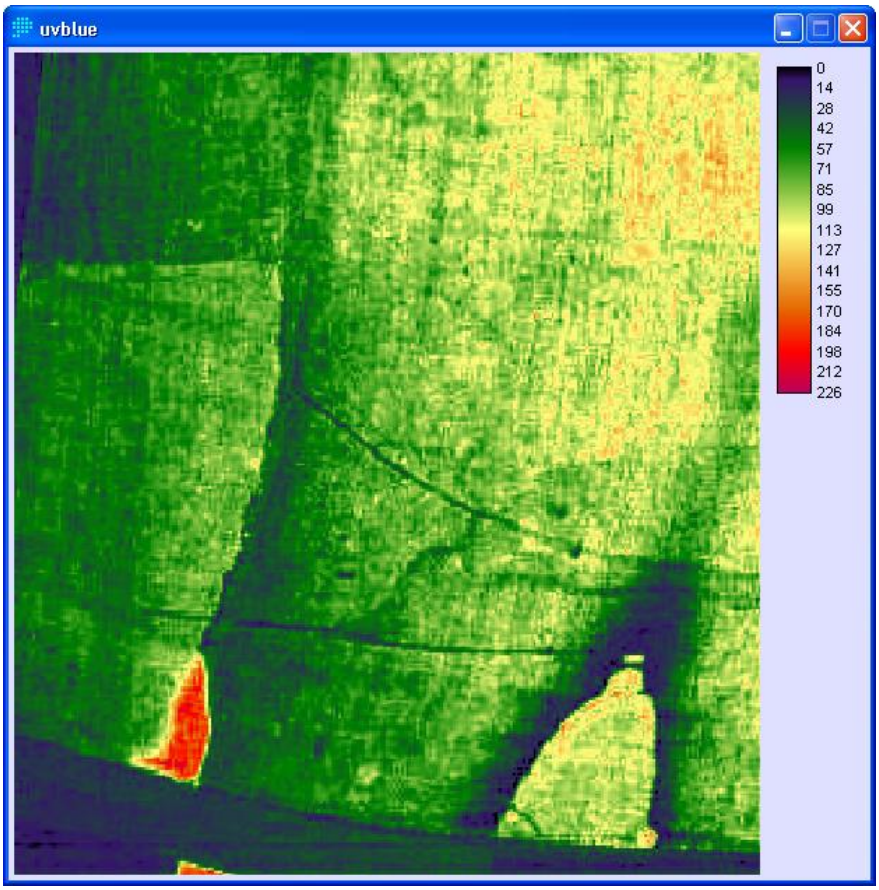

Figure 2. Blue band extracted from the clipped version of the UV-F image.

Average z-score values were then calculated for each image object in Figure 14. The average z-score values for image objects were then mapped using a unipolar (ramp from white) palette. The resultant image (Figure 15) provides another way to visualize the anomalous nature of the C-14 sample area.

Finally, a graph was developed for values of the first component of the PCA along a profile line (transect) running transverse to and across the seam joining the cotton patch to the TS. The profile line extends from the pixel at row/column coordinates 13/170 (upper left) to the pixel at row/column coordinates 160/217 (upper right) (Figure 16). The graph (Figure 17) shows values of the first component of the PCA along the profile line. The profile line is 152 pixels in length and crosses the seam at pixel 74.

RESULTS AND DISCUSSION

The image processing techniques used to investigate the UV-F photograph provide both image and tabular data supporting discussion of several important issues related to the C-14 sample area of the TS.

Ultraviolet fluorescence (UV-F) photography

In recent years, art historians have used UV-F photography for forensic analysis of paintings (Hain et al., 2003; Thoury et al., 2005; Anonymous, 2003). UV-F photography which can be taken today with the use of a digital camera, a UV filter for the digital camera lens, and a UV light source measures visible fluorescence induced by UV radiation. Any material that is sensitive to UV light will fluoresce. Different painting materials (paints, pigments, varnishes, dyes, etc.) will exhibit different fluorescence when exposed to UV light and will emit visible light (Hain et al., 2003; Thoury et al., 2005; Anonymous, 2003). It was the emitted visible light induced by UV radiation of the TS that was captured by the UV-F photograph (Rogers, 2004).

Newer applied paints and varnish layers under UV light will fluoresce less than older materials (Hain et al., 2003; Thoury et al., 2005; Anonymous, 2003). Therefore, retouched (dyed) areas will appear darker in a UV-F image. With regard to the UV-F photograph of the C-14 sample area, Rogers observed: “The small, triangular, white area is where the Raes sample was cut in 1973. The radiocarbon sample was cut upward from there about 1 cm to the right of the seam and about 7 cm long. The area where the radiocarbon sample was taken is relatively dark, a fact that is not the result of dirt, image color, or scorching. The cloth is much less fluorescent in that area, brightening into more typical fluorescence to the right. The photograph proves that the radiocarbon

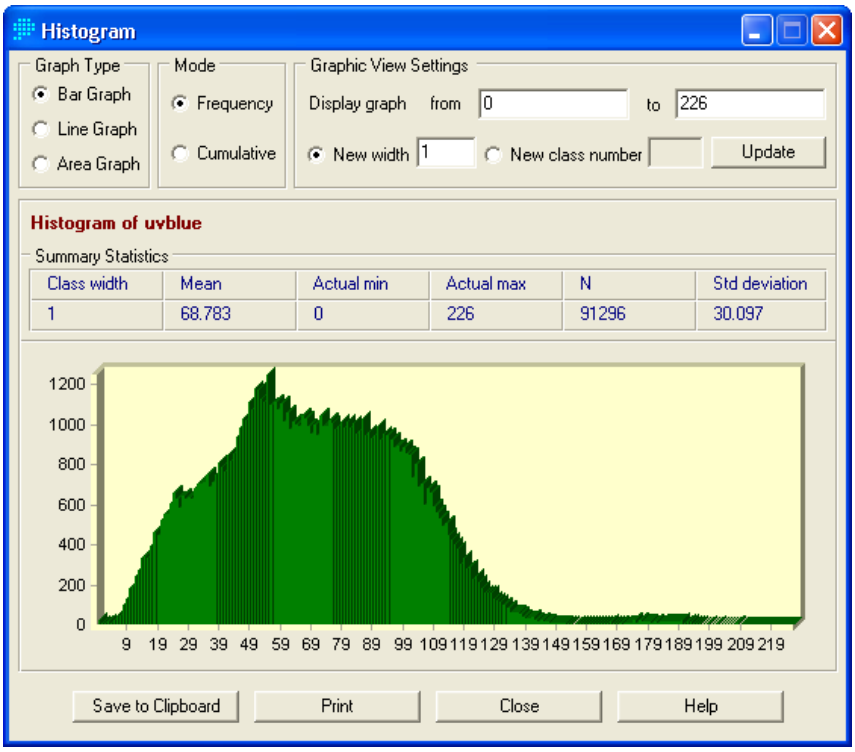

Figure 3. Histogram of blue band extracted from the clipped version of the UV-F image.

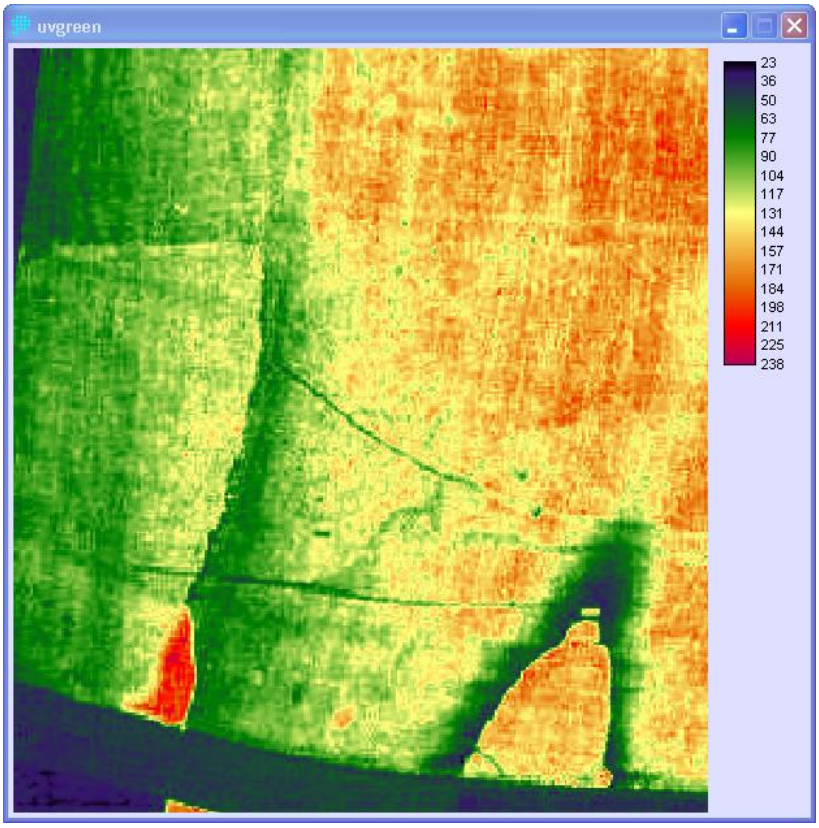

Figure 4. Green band extracted from the clipped version of the UV-F image.

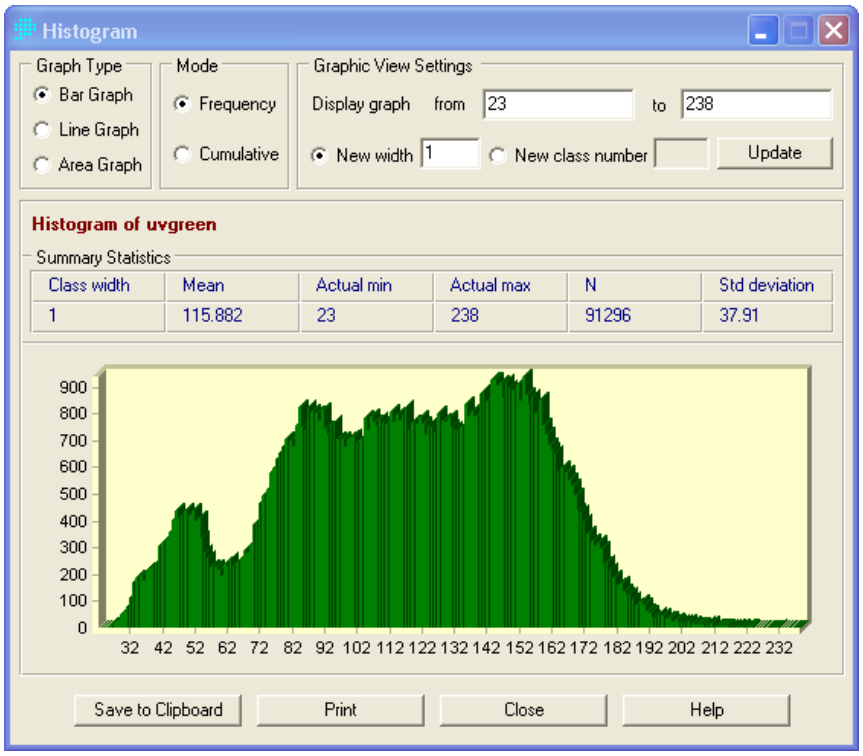

Figure 5. Histogram of green band extracted from the clipped version of the UV-F image.

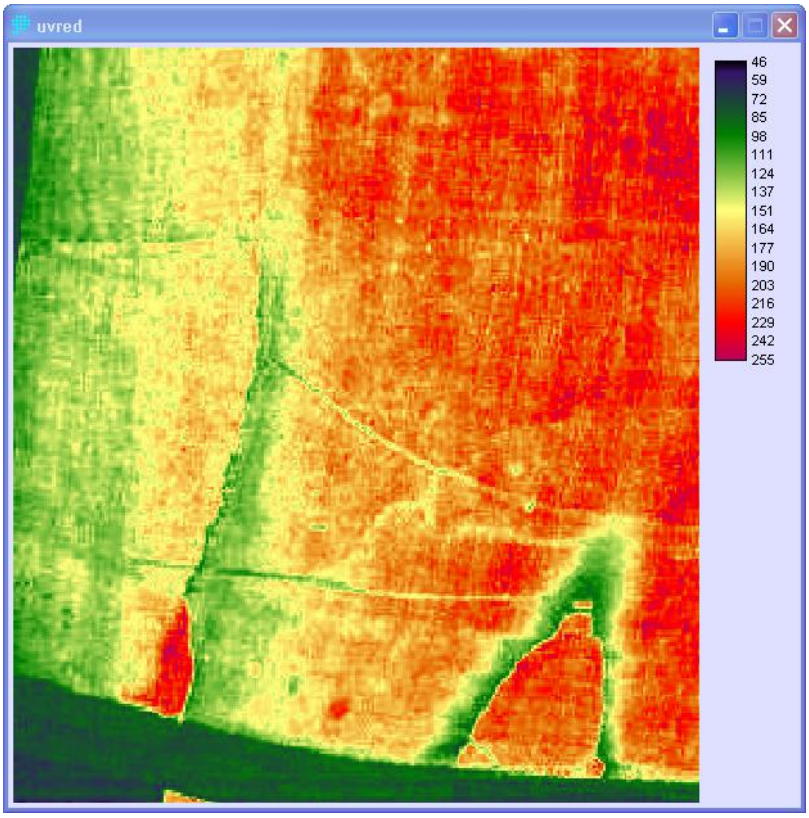

Figure 6. Red band extracted from the clipped version of the UV-F image.

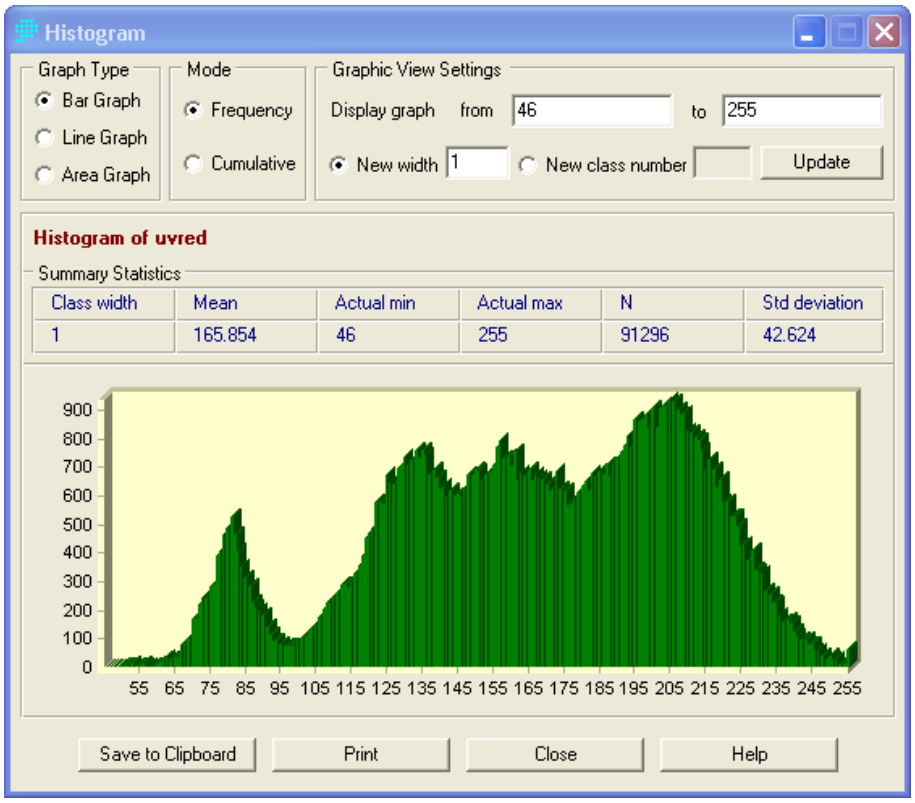

Figure 7. Histogram of red band extracted from the clipped version of the UV-F image.

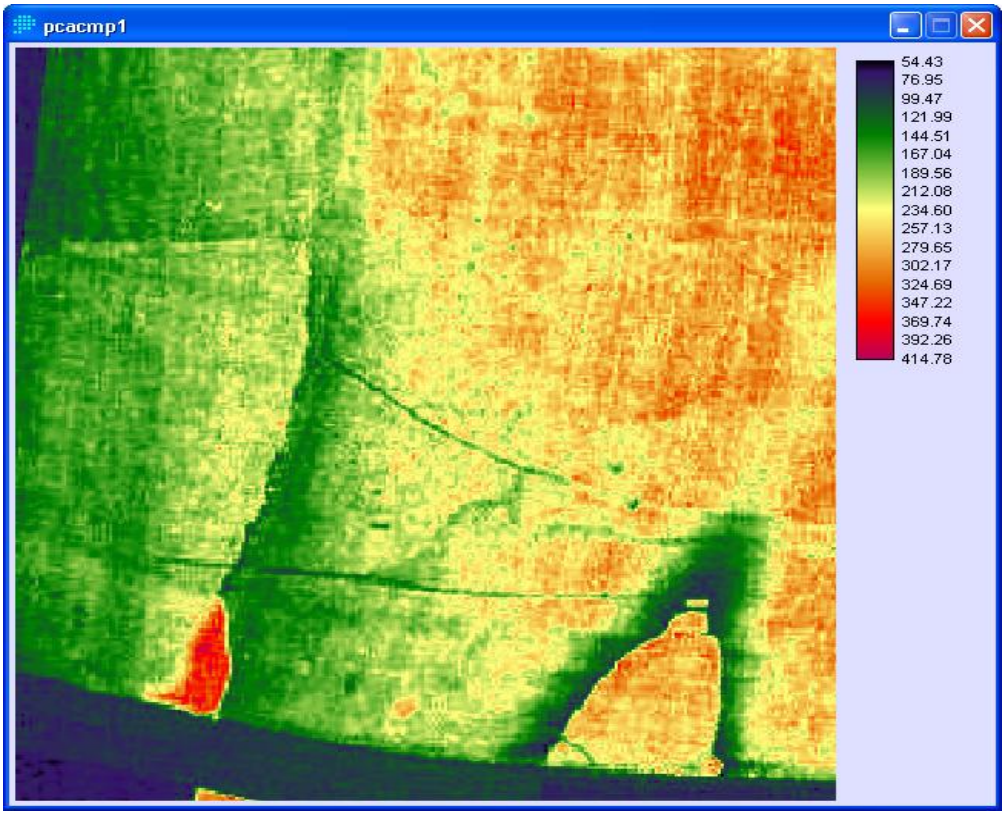

Figure 8. First component of the PCA.

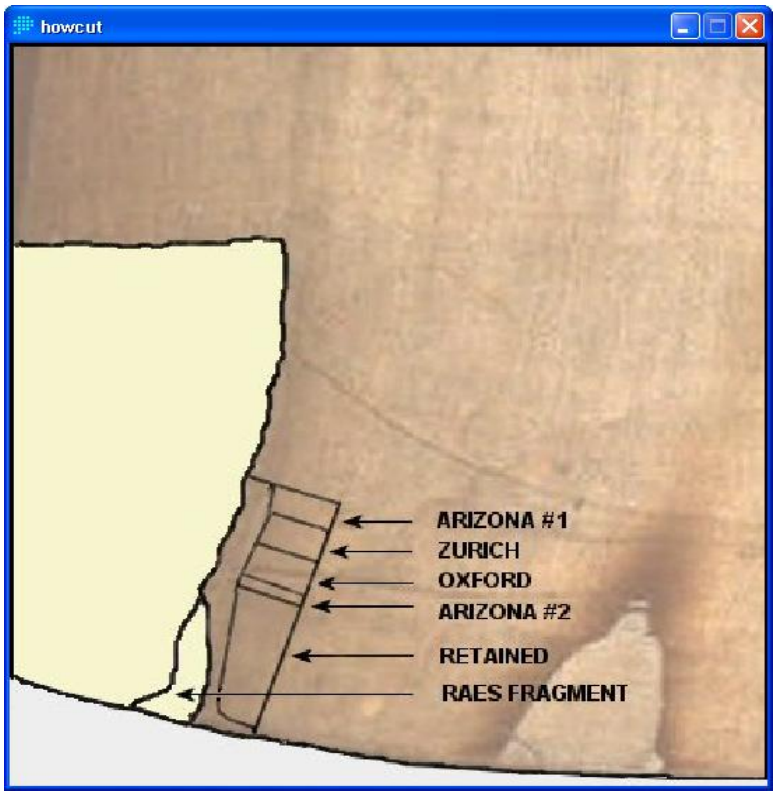

Figure 9. Benford and Marino graphic of C-14 sample area [4].

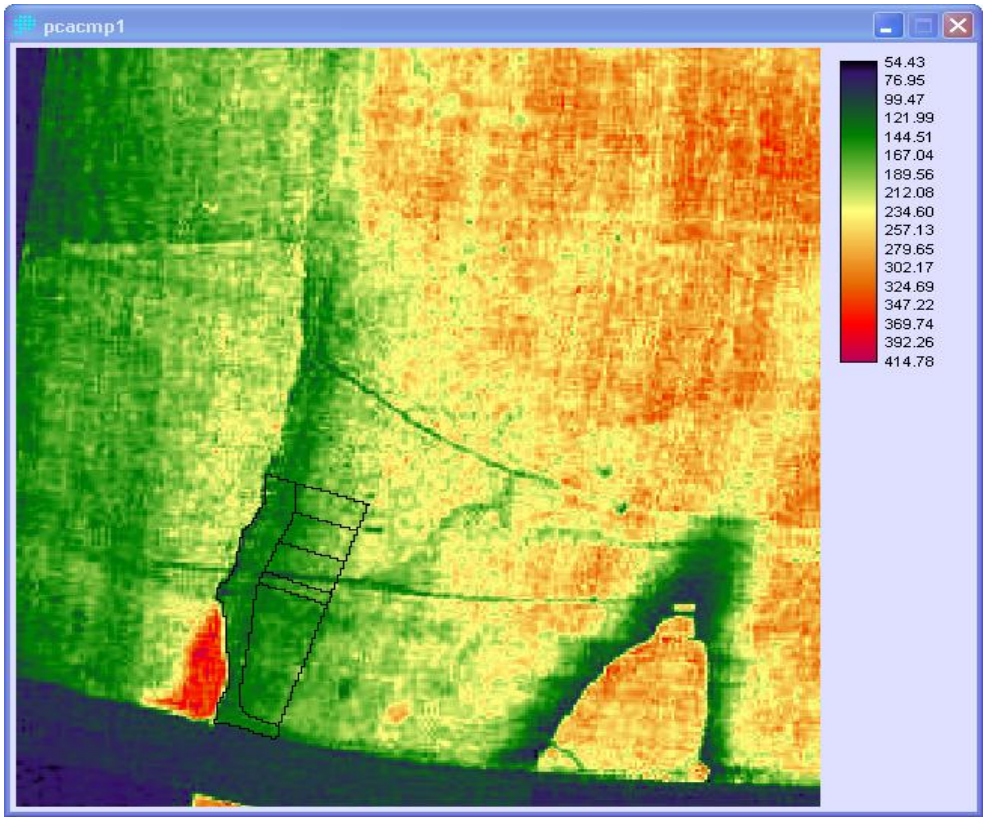

Figure 10. First component of the PCA with overlay of the C-14 sample area.

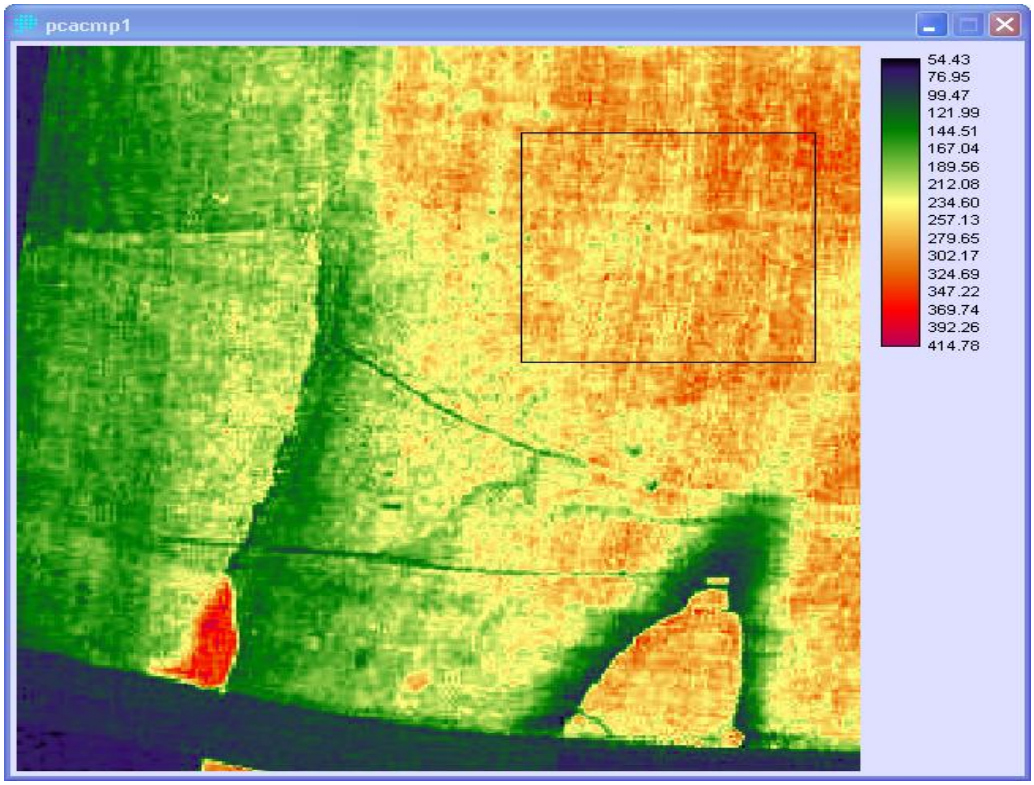

Figure 11. First component of the PCA with overlay of the z-score sample area.

Table 1. Selected statistics of the first component of the PCA for the Z-score sample area.

Statistic	Z-score sample area
Minimum value	167.4316
Maximum value	370.0649
Mean	276.7864
Standard deviation	24.6465
Number of pixels	10,000

area has a different chemical composition than the main part of the cloth. This was obviously not considered before the sample was cut." (http://www.shroudstory.com/faq/turin-shroud-faq-05.htm).

Figures 2, 4 and 6 show the brightness values for the 8-bit blue, green, and red bands extracted from the 24-bit RBG UV-F image. Each of the 8-bit images virtually confirms Rogers' observation with regards to the fluorescence of the UV-F image. That is, the brightness values are lower in the area where the C-14 samples were taken and are higher to the right. The brightness values for each image range from 0 to 255 and are shown in the legend on the right hand side of each image. Rogers' observation is further confirmed by the image of the first component of the PCA (Figure 10), an image created by statistically "compressing" the blue, green, and red bands extracted from the 24-bit UV-F image.

The graph of brightness values of the first component of the PCA in Figure 17 provides an interesting way of visualizing the change in brightness values in the image noted by Rogers. Note that the brightness values increase from the starting point of the profile line to where the profile line crosses the seam (pixel 74). At that point, the brightness values decrease dramatically and then increase from the seam to the ending point of the profile line. The profile line enters and exits the Zurich sample (Area 2) at pixels 87 and 109, respectfully. The cotton patch and C-14 sample area fluoresce differently than the rest of the TS.

Spectrally anomalous nature of the C-14 sample area

The first component of the PCA (Figure 11) was used to calculate the z-score for each pixel in the UV-F photograph. Other researchers have used the UV-F photograph to qualitatively assess the anomalous nature of the sample area. Based on pixel z-scores (Figure 12), the area where the C-14 sample area is located is anomalous when compared to the upper right portion of the UV-F image (the area UV-F photograph above the area charred in the 1532 C.E fire). The C-14 sample areas (Areas 1 through 4) have average z-score values ranging from -4.8327 to -3.9807 (Table 2).

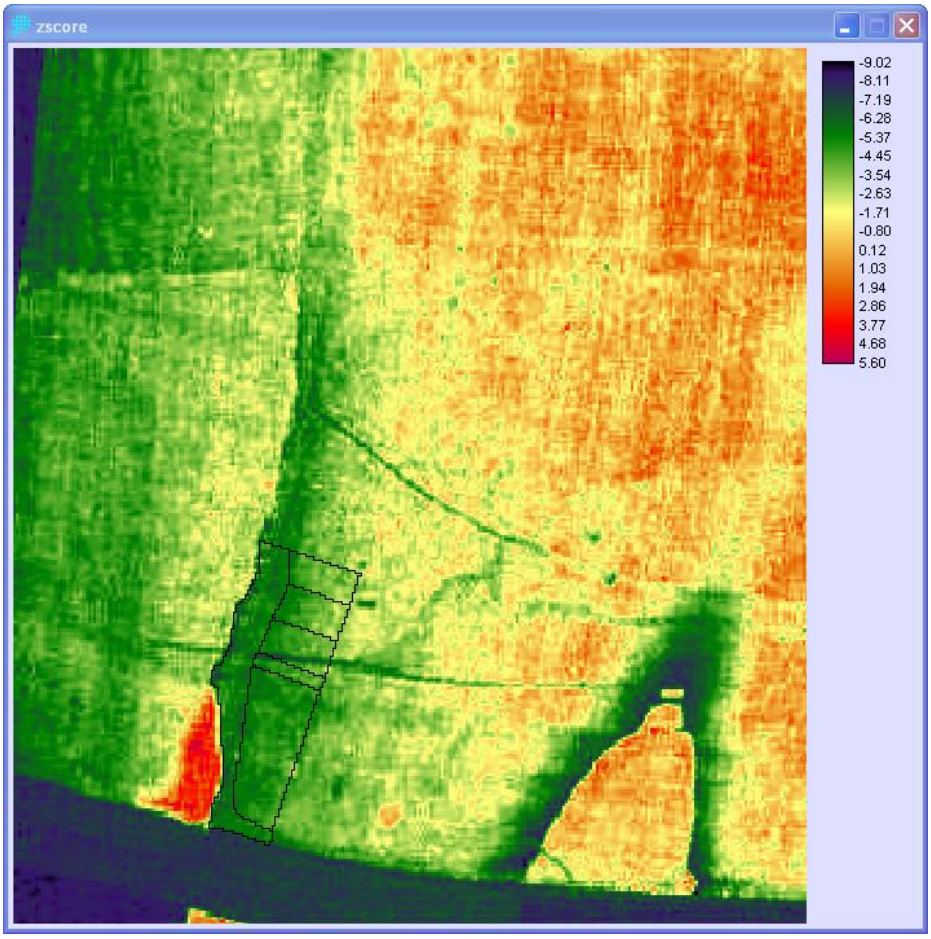

Figure 12. Z-score image calculated from the first component of the PCA with overlay of the C-14 sample area.

A one-sample z-test was used to determine whether the four C-14 areas are statistically different when compared to the upper right portion of the TS (the z-score sample area). This statistic compares the mean of a set of measurements (the mean z-scores for the four C-14 sample areas) to a given constant (the mean z-score for the z-score sample area). Two hypotheses were postulated for the one-sample z-test.

H_0: There is no significant difference between the mean z-score for the z-score sample area and the sample means for the four C-14 sample areas, or $\mu = \chi$ (where μ is the population mean and χ is the sample mean).

H_1: There is a significant difference between the mean z-score for the z-score sample area and the sample means for the four C-14 sample areas, or $\mu \neq \chi$ (where μ is the population mean and χ is the sample mean).

The rejection criteria were based on a significance level of 0.05 alpha (95% confidence interval) with a two-tailed test. The test statistic for the z-test is defined by the following equation:

$$z = \frac{\chi - \mu}{\frac{\sigma}{\sqrt{n}}}$$

Where, χ is the z-score sample mean, μ is the population mean, σ is the population standard deviation, and n is the sample size. The population mean and the population standard deviation for the z-score sample area were -2.3084 and 0.9999, respectively (Table 2). Other data used in the calculation of the one sample z-test, and the results of the z-test statistic calculation, are included in Table 3. The critical values for the z-test score were -1.96 and 1.96.

Because the z-test scores for the four C-14 sample areas are significantly less than -1.96, the null hypothesis (H_0) was rejected for all four C-14 sample areas. There are significant differences between the mean z-score for the z-score sample area and the sample z-score means for the four C-14 sample areas. Spectrally, the four C-14 sample areas are statistically anomalous when compared to the z-score sample area, the portion of the UV-F image with fluorescence that is more typical of the TS.

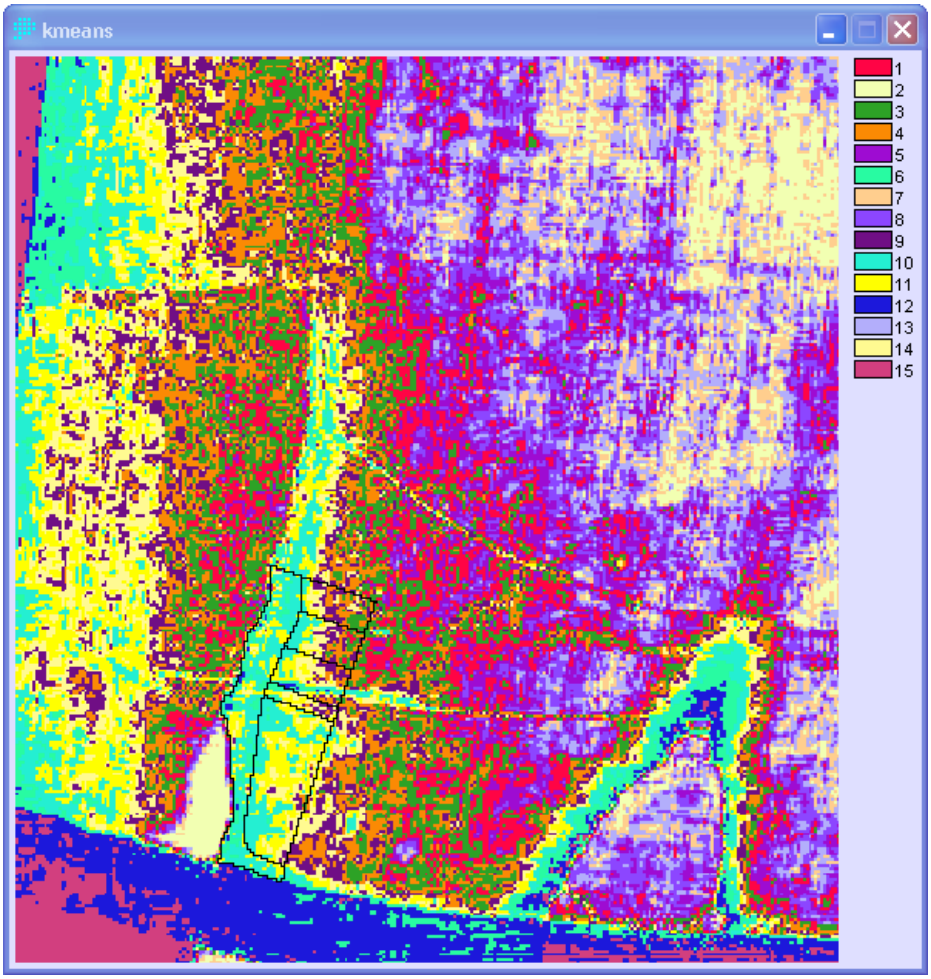

Figure 13. C-14 sample area (vector) overlayed on the KMEANS classification calculated from the first component of the PCA.

Observed gradients in the C-14 sample area

Several researchers have noted the presence of "gradients" in the radiocarbon dating area based on different amounts of C-14 in the four samples. Walsh (1999) determined that "higher levels of ^{14}C were measured at increasing distance from the edge of the Shroud linen." He based his findings on linear regression analysis of subsample radiocarbon dates with the corresponding distance of the sample to the edge of the TS. Marino and Benford (2000) used the three laboratory dates and Walsh's regression line to estimate dates for the four C-14 samples. The trend of the gradient of the z-score sample means for the four C-14 samples is consistent with the trend of the age gradient reported by the three C-14 laboratories in 1988 (Damon et al., 1989) and the trend of the age gradient estimated by Marino and Benford (2000) (Table 4).

Marino and Benford (2000) provided calendar dates for the four sample areas (1238, 1246, 1326, and 1430) in their article. The calendar dates were converted to ages by subtracting 1989 (the publication date of the *Nature* article with the radiocarbon dates) from each calendar date. As Marino and Benford noted in their article, The Arizona #1 (Area 1) and Arizona #2 (Area 4) samples were reported as one radiocarbon age estimate. They also noted that they were unable to separate the measurements for the two Arizona samples from the laboratory data (Damon et al., 1989).

The UV-F image used in this investigation provided the means for identifying differences in the chemical composition of the TS. It can be posited, given the preceding discussion regarding the use of UV-F photography, that the UV-F brightness values recorded information about the dyed and non-dyed portions of the TS. As Rogers concluded, the medieval restorer applied dyes to the 16th century cotton patch and TS linen to match the aged appearance of the TS: "The presence of alizarin dye and red lakes in the Raes and radiocarbon samples indicates that the color has been manipulated. Specifically, the color and distribution of the coating implies that repairs were made at an unknown time with foreign linen dyed to

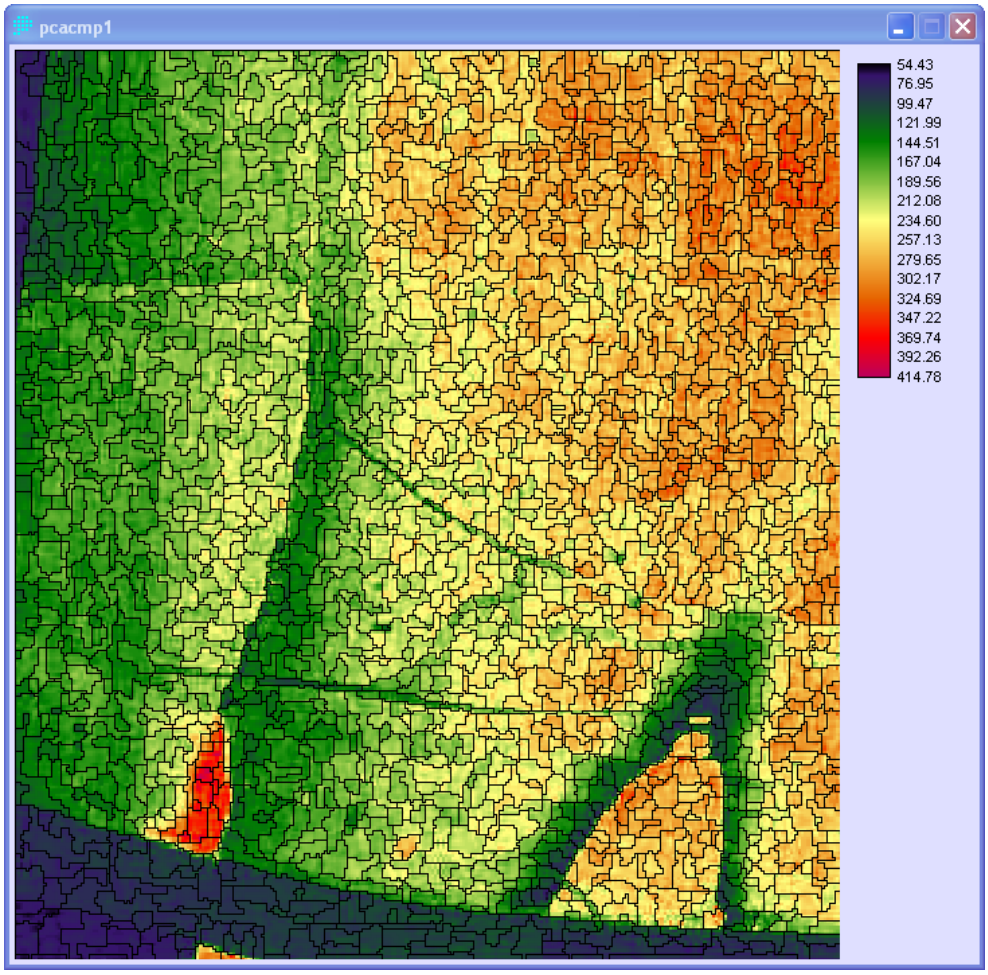

Figure 14. Image objects overlayed on the first component of the PCA.

match the older original material. Such repairs were suggested by Benford and Marino" (Rogers, 2005).

Given the spatial resolution of the UV-F image, individual threads on either side of the seam where Benford and Marino (2008) have postulated the cotton patch was rewoven into the TS could not be discriminated via image processing. However, the image created via K-MEANS classification (Figure 13) shows what appears to be the twill pattern of the TS in the upper right hand portion of the image. Availability of higher spatial resolution imagery in the future may enable discrimination of individual threads of the cotton patch and the TS linen via digital image processing.

Conclusions

The digital image processing techniques described in this paper to process the UV-F photograph can be used to ensure that any future radiocarbon dating of the TS is based on samples taken from areas that are representative (statistically similar) to that of the TS. More importantly, this paper demonstrates that digital image processing provides new techniques and tools for non-destructive investigation of the TS. These include tools for enhanced visualization and analysis of multispectral TS imagery. There may be as yet unknown information hidden in the TS that can be identified via digital image processing of multispectral TS imagery. For example, the red band extracted from the UV-F image (Figure 6) shows features that are otherwise not apparent in the UV-F photograph. Additional digital image processing of the UV-F image may also produce other new information.

Benford and Marino (2008) demonstrated that the C-14 samples were taken from an area of the TS that had been expertly restored by medieval artisans by reweaving a cotton patch into the original linen of the TS. According to Brown (2005), the artisans then attempted to dye the newly rewoven area to match the aged appearance of the remainder of the TS. The image segments created using the first component of the PCA (Figure 14) may provide a way to identify unique chemical composition features on the TS. Also, the unsupervised classification image produced via K-MEANS clustering (Figure 13) may provide a

Figure 15. Average z-score values for each image object.

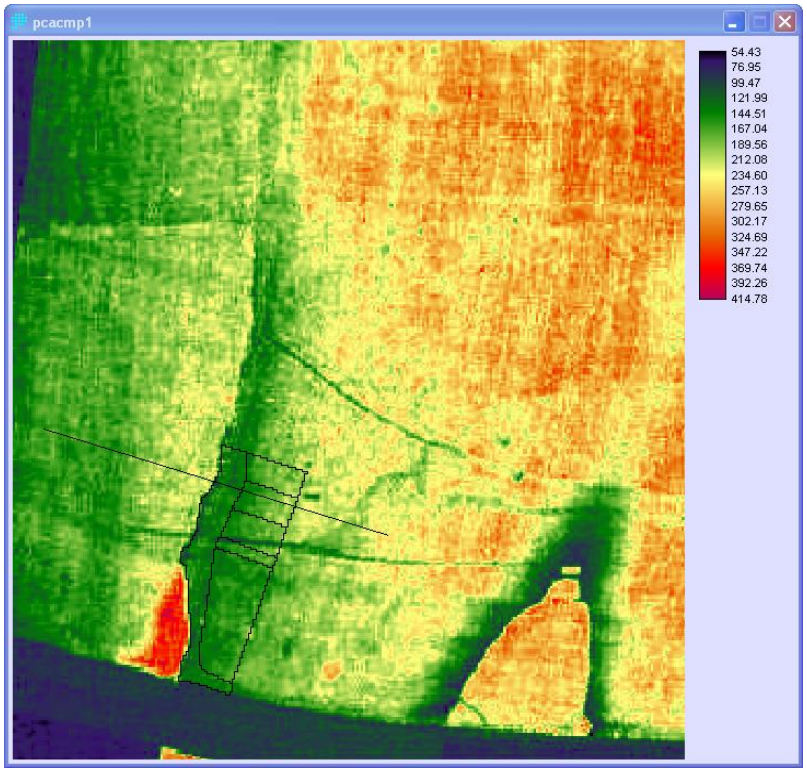

Figure 16. C-14 sample area (vector) and profile line (vector) overlayed on the first component of the PCA.

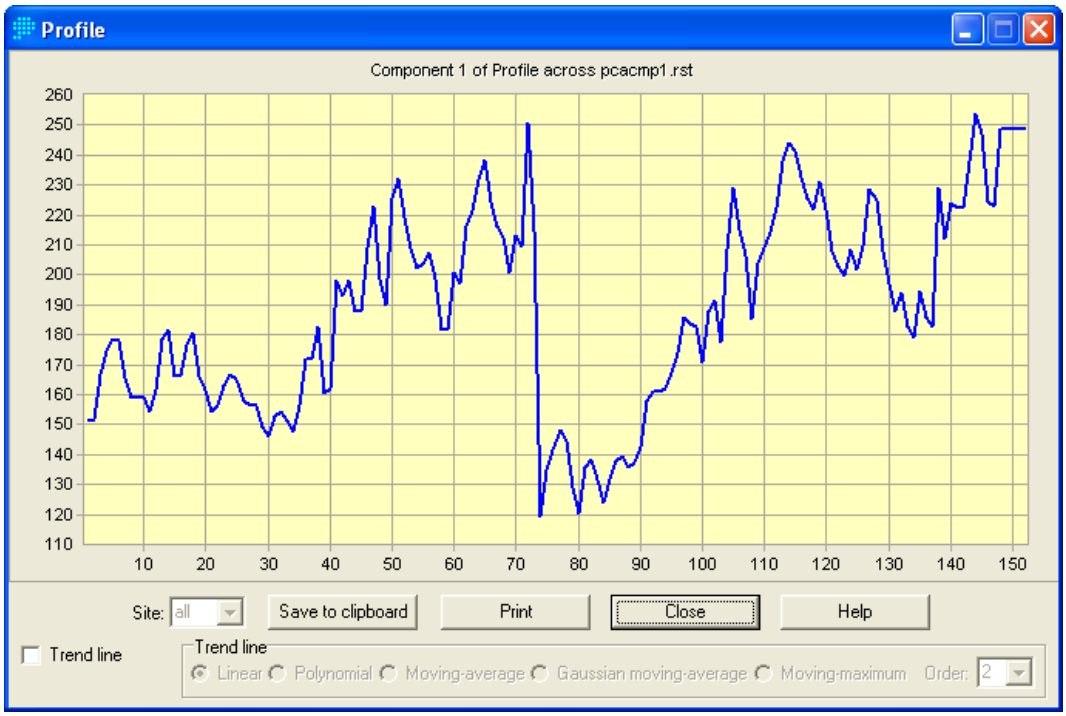

Figure 17. Graph of brightness values along the profile line shown in Figure 16.

Table 2. Selected statistics of the z-scores for the four C-14 sample areas and the Z-score sample area.

Statistic	Area 1[1]	Area 2[1]	Area 3[1]	Area 4[1]	Z-score sample area
Minimum value	-6.2182	-5.9697	-7.2742	-6.9094	-4.4367
Maximum value	-1.9081	-1.9382	-2.4983	-3.5189	3.7845
Mean	-3.9807	-4.2483	-4.8312	-4.8327	-2.3084
Standard deviation	0.8044	0.9843	0.9162	0.7726	0.9999
Number of pixels	298	328	351	128	10,000

[1]Area 1 is the area shown in Figure 9 as Arizona #1, Area 2 is the area shown as Zurich, Area 3 is the area shown as Oxford, and Area 4 is the area shown as Arizona #2.

Table 3. One sample Z-Test (Mean Z-Score for the Z-Score Sample Area and the Z-Score Sample Means for the Four C-14 Sample Areas)

Statistic	Area 1	Area 2	Area 3	Area 4
n	298	328	351	128
Z-score sample mean (χ)	-3.9707	-4.2483	-4.8312	-4.8327
Z-test score	-28.6986	-35.1366	-47.2694	-28.5621
Test result	Reject H_0	Reject H_0	Reject H_0	Reject H_0

Table 4. Age of C-14 Sample Dates and the Sample Means for the Four C-14 Sample Areas

C-14 Sample	C-14 laboratory ages	Marino and Benford ages[1]	Z-score sample means
Arizona #1 (Area 1)	646 ± 31	559	-3.9707
Zurich (Area 2)	676 ± 24	663	-4.2483
Oxford (Area 3)	750 ± 30	743	-4.8312
Arizona #2 (Area 4)	Not reported	751	-4.8327

way to identify the exact area where the cotton patch and the portion of the TS adjacent to the cotton patch was dyed to match the older linen material of the TS.

RECOMMENDATIONS

One academic discipline apparently not represented among the Shroud of Turin Research Project (STURP) investigators was that of geography. As a geographer who is new to TS research, the author would like to make several recommendations based on the investigation of the UV-F photography of the C-14 sample area described in this paper.

First, new multispectral digital imagery should be taken for both the dorsal and ventral sides of the TS. These images should be taken at the highest possible spatial, spectral, and radiometric resolutions, an idea suggested previously by Fanti (1997). Further, any multispectral (x-ray, ultraviolet, visible, and infrared) images taken of the TS should be geospatially referenced to one another. In other words, the pixels in one image should match those in all of the other images. Taking digital imagery will not harm the TS in any way. More importantly, the availability of high resolution imagery will enable researchers to undertake other non-destructive investigations of the TS. As demonstrated in this paper, the UV-F photograph of the C-14 sample area of the TS encodes information that previously was unknown to TS researchers. There may be other information hidden within the TS that is waiting to be identified via digital image processing of higher resolution imagery.

Second, as has been suggested by other researchers (Latendresse, 2010), a planar coordinate system should be established for the TS. Ideally, the coordinate system should be based on pixel coordinates measured from the upper left corner of digital images for both the dorsal and ventral sides of the TS.

This would be a Cartesian Quadrant IV coordinate system modified for use with digital image processing and mapping software. The Shroud coordinate system would measure pixel coordinates for both the x-axis (columns) and y-axis (rows) using positive values. This would enable TS researchers to georeference their work so that their findings could be compared to those of other researchers. It would also enable development of a gazetteer (geographic index) of TS features such as blood and serum stains and burn marks. More importantly, high resolution (spatial, spectral, and radiometric) imagery tied to a consistent coordinate system will create in a “TS map” that would serve as a “common operating picture” for future collaborative TS research.

ACKNOWLEDGEMENTS

The author would like to thank Barrie Schwortz, Ray Schneider, Giulio Fanti, and Joe Marino for their assistance and encouragement. They freely donated their time to help me start my investigation to determine if the digital image processing techniques used by the land remote sensing community could provide new, relevant, scientifically-derived information about the TS. The author also thanks his wife, Bobby, for her continuing support and encouragement.

SUPPORTIVE/SUPPLEMENTARY MATERIAL

The author will make copies of the raster and vector data used for this investigation available upon email request. Raster data will be provided in .tif format; vector data will be provided in Esri shapefile format.

REFERENCES

Anonymous (2003). The use of ultraviolet induced visible-fluorescence in the examination of Museum Objects, Part II. Conservation O Gram (U.S. National Park Service) 1/10, 1-4.

Avis C, Lynn D, Lorre J, Lavoie S, Clark J, Armstrong E, Addington J (1982). In: Image Processing of the Shroud of Turin, 1982 Proceedings of the IEEE International Conference on Cybernetics and Society, pp. 554-558.

Benford MS, Marino JG (2008). Discrepancies in the radiocarbon dating area of the Turin shroud. Chem. Today 26: 4-11.

Brown JL (2005). Microscopical investigation of selected Raes threads from the Shroud of Turin, http://www.shroud.com/pdfs/brown1.pdf.

Clark Labs, IDRISI GIS and Image Processing Software, http://www.clarklabs.org.

Damon PE, Donahue DJ, Gore BH, Hatheway AL, Jull AJT, Linick TW, Sercel PJ, Toolin LJ, Bronk CR, Hall RE, Hedges M, Housley R, Law IA, Perry C, Bonani G, Trumbore S, Woelfli W, Ambers JC, Bowman SGE, Leese MN, Tite MD, (1989). Radiocarbon dating of the Shroud of Turin, Nature 337(6208): 611-615.

Environmental Systems Research Institute (Esri) Web site, http://www.esri.com.

Fanti GA (1997). Proposal for high resolution colorimetric mapping of the Turin Shroud: Analysis of metrological problems, http://www.shroud.com/fanti.htm.

Hain M, Bartl J, Jacko V (2003). Multispectral analysis of cultural heritage artifacts. Measurement, Sci. Rev. 3:9-12.

Jensen JR (1996). Introductory digital image processing: A remote sensing perspective, 2nd ed. Prentice Hall: Upper Saddle River, NJ.

Latendresse M (2010). Shroud Scope: A web tool to analyze high-resolution photographs of the Shroud of Turin, Proceedings of the international workshop on the scientific approach to the Acheiropoietos images, http://www.acheiropoietos.info/proceedings/proceedings.php.

Marino J, Benford MS (2000). Evidence for the skewing of the C-14 dating of the Shroud of Turin due to repairs, http://www.shroud.com/pdfs/marben.pdf.

Rogers RN (2004). Frequently asked questions (FAQs), http://www.shroud.com/pdfs/rogers5faqs.pdf.

Rogers RN (2005). Studies on the radiocarbon sample of the Shroud of Turin. Thermochimica Acta, 425:189-194.

Rogers RN, Arnoldi A (2000). Scientific method applied to the Shroud of Turin: A review, http://www.shroud.com/pdfs/rogers2.pdf.

Shroud of Turin skeptical spectacle, Web site, http://www.skepticalspectacle.com/carbon1400.htm.

Ray Rogers. Frequently asked question (FAQ): Shroud story, http://www.shroudstory.com/faq/turin-shroud-faq-05.htm.

Thoury M, Elias M, Frigerio JM, Barthou C (2005). In non-destructive identification of varnishes by UV fluorescence spectroscopy, Proceedings of the SPIE (Optical Methods for Arts and Archaeology), pp. 151-161.

Walsh B (1999). In: The 1988 Shroud of Turin radiocarbon tests reconsidered, Proceedings of the 1999 Shroud of Turin International Research Conference, 1999, pp. 326-342.